Amorphous thin film growth: Effects of density inhomogeneities

Martin Raible, Stefan J. Linz, and Peter Hänggi
Theoretische Physik I, Institut für Physik, Universität Augsburg, D-86135 Augsburg, Germany
(Received 23 February 2001; published 30 August 2001)

A nonlinear stochastic growth equation for the spatiotemporal evolution of the surface morphology of amorphous thin films in the presence of potential density variations is derived from the relevant physical symmetries and compared to recent experimental results. Numerical simulations of the growth equation exhibit a saturation of the surface morphology for large film thickness originating from the inclusion of the density inhomogeneities. Furthermore, we argue why moundlike surface structures observed on vapor deposited amorphous films are not the result of the Grinfeld instability.

DOI: 10.1103/PhysRevE.64.031506 PACS number(s): 61.43.Dq, 68.35.Bs

I. INTRODUCTION

Recently, there has been increasing interest in the understanding of the kinetics of surface growth processes (e.g., see in Ref. [1]). The evolution of the surface morphology, as it appears in molecular beam epitaxy or physical vapor deposition experiments is determined by the interplay of the deposition of particles and surface diffusion effects that result in a competition between surface roughening and smoothening processes [2–6]. Experimental studies on *amorphous thin films* deposited by electron beam evaporation exhibit the formation of a moundlike surface structure on a mesoscopic length scale [7–11]. Despite the complexity of the growth process on an atomic scale, this indicates that continuum models based on stochastic field equations [1] serve as a useful tool for the understanding of the kinetics of amorphous thin film growth.

The typical form of such a stochastic growth equation is given by

$$\partial_t H = G[\vec{\nabla} H] + F + \eta, \tag{1}$$

where $H(\vec{x},t)$ represents the height of the surface above a given substrate position $\vec{x}$ (see Fig. 1). $G[\vec{\nabla} H]$ comprises all surface relaxation processes, F denotes the mean deposition rate, and η is the deposition noise that represents the fluctuations of the deposition around its mean F. These fluctuations are assumed to be Gaussian white, i.e.,

$$\langle \eta(\vec{x},t)\rangle = 0; \quad \langle \eta(\vec{x},t)\,\eta(\vec{y},t')\rangle = 2D\,\delta^2(\vec{x}-\vec{y})\,\delta(t-t'), \tag{2}$$

where the brackets denote ensemble averaging and D the fluctuation strength. Transformation in a frame comoving with the deposition rate F, $h(\vec{x},t) = H(\vec{x},t) - Ft$, yields the equation

$$\partial_t h = G[\vec{\nabla} h] + \eta. \tag{3}$$

The functional form of $G[\vec{\nabla} h]$ can be obtained by using the physical symmetries governing the growth process. In the context of *amorphous* thin film growth, these symmetries are translational invariance in space and time and rotational and mirror invariance in the plane perpendicular to the growth direction, cf. Fig. 1. An additional symmetry principle that we have applied in a recent study [12] was the condition of no excess velocity. This means that the functional $G[\vec{\nabla} h]$ can be written in the form $G[\vec{\nabla} h] = -\vec{\nabla}\cdot\vec{j}$. By using these symmetries we proposed the stochastic growth equation [12,13]

$$\partial_t h = a_1 \vec{\nabla}^2 h + a_2 \vec{\nabla}^4 h + a_3 \vec{\nabla}^2 (\vec{\nabla} h)^2 + \eta, \tag{4}$$

with a_1, a_2, a_3 being negative as the minimal model equation for amorphous thin film growth in the absence of excess velocity.

In the light of a recent comparison to experimental data [14] the condition of no excess velocity needs to be reexamined. It is only fulfilled if (i) particle desorption does not occur, i.e., no particles leave the surface, and if (ii) the film growth takes place with constant density ρ_0. While in fact particle desorption is negligible during the growth of amorphous films since it requires much higher energies, the assumption of film growth with density variations cannot be excluded *a priori*. Moreover, a careful comparison of Eq. (4) with experimental results for amorphous $Zr_{65}Al_{7.5}Cu_{27.5}$ film growth [14] has indicated the necessity of the inclusion of density inhomogeneities. These density variations result in an additional term of Kardar-Parisi-Zhang form [15] in the deposition equation, yielding

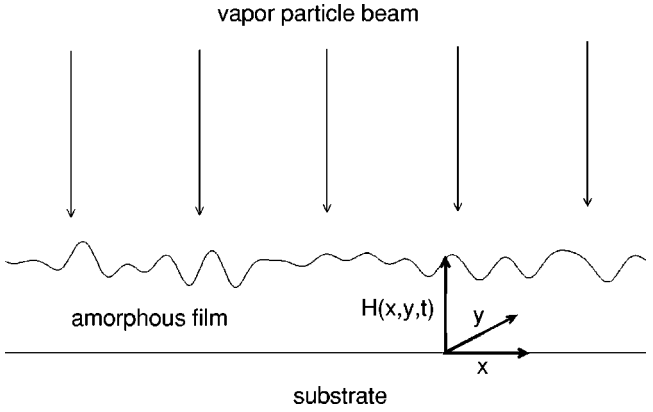

FIG. 1. Sketch of the vapor deposition of an amorphous film on a substrate.

$$\partial_t h = a_1 \vec{\nabla}^2 h + a_2 \vec{\nabla}^4 h + a_3 \vec{\nabla}^2 (\vec{\nabla} h)^2 + a_4 (\vec{\nabla} h)^2 + \eta, \quad (5)$$

with a_4 being positive [12,13].

The previous work [12] was restricted to a detailed analysis of Eq. (4) and our comparison of Eq. (5) with the experimental results [14] was also limited by the available data and the chosen material. Hence, there is a need for a thorough investigation of Eq. (5) with the inclusion of density inhomogeneities. In the Appendix, we also address the question whether the pattern forming processes in vapor deposited amorphous films might be, alternatively, interpreted as the consequence of a Grinfeld instability.

II. MODEL

In this section, we first present a coherent derivation of the simplest functional form of the stochastic field equation using the symmetry principles governing the growth of amorphous films. Subsequently, we relate the constituents of this equation to the underlying microscopic processes.

The absence of particle desorption implies a balance equation

$$\partial_t c = \rho_0 [- \vec{\nabla} \cdot \vec{j} + F + \eta], \quad (6)$$

where $c(\vec{x},t)$ denotes the number of atoms of the amorphous film per substrate area above a given substrate position $\vec{x}$. Here, the current $\vec{j}$ is given by the combination of all surface relaxation processes. Mass transport inside the amorphous material can be neglected. Invariance under translation in time and space rules out any explicit appearance of time t, space coordinate $\vec{x}$ or height H in $-\vec{\nabla} \cdot \vec{j}$. Therefore, the corresponding functional $G_c[\vec{\nabla} H] = -\vec{\nabla} \cdot \vec{j}$ for the concentration c depends only on gradients and higher spatial derivatives of the height function $H(\vec{x},t)$. Moreover, the isotropy of the amorphous phase implies rotational and mirror invariance in the plane perpendicular to the growth direction, cf. Fig. 1. Therefore, $G_c[\vec{\nabla} H]$ must be a scalar under these transformations. By using the afore-mentioned symmetries we expand the possible terms of $G_c[\vec{\nabla} H]$ in a power series of $\vec{\nabla}$ and $\vec{\nabla} H$ up to $\mathcal{O}(\vec{\nabla}^3, (\vec{\nabla} H)^2)$ and obtain the functional form

$$G_c(\vec{\nabla} H) = a_1 \vec{\nabla}^2 H + a_2 \vec{\nabla}^4 H + a_3 \vec{\nabla}^2 (\vec{\nabla} H)^2 + a_5 M \quad (7)$$

with

$$M = \det \begin{pmatrix} \partial_x^2 H & \partial_y \partial_x H \\ \partial_x \partial_y H & \partial_y^2 H \end{pmatrix}, \quad (8)$$

or, equivalently the continuity equation

$$\partial_t c = \rho_0 [a_1 \vec{\nabla}^2 H + a_2 \vec{\nabla}^4 H + a_3 \vec{\nabla}^2 (\vec{\nabla} H)^2 + a_5 M + F + \eta]. \quad (9)$$

Allowing for density variations depending on the surface inclination, the rate of change of c is related to the rate of change of H by $\partial_t c = \rho(\vec{\nabla} H) \partial_t H$. Here $\rho(\vec{\nabla} H)$ denotes the density of the film close to the surface. Dividing Eq. (9) by $\rho(\vec{\nabla} H)$ leads to

$$\partial_t H = \frac{\rho_0}{\rho(\vec{\nabla} H)} [a_1 \vec{\nabla}^2 H + a_2 \vec{\nabla}^4 H + a_3 \vec{\nabla}^2 (\vec{\nabla} H)^2 + a_5 M + F + \eta]. \quad (10)$$

The density variations can then be expanded in the gradients of H yielding $[\rho(\vec{\nabla} H)]^{-1} = \rho_0^{-1} [1 + (a_4/F)(\vec{\nabla} H)^2 + \mathcal{O}((\vec{\nabla} H)^4)]$ with a_4 being necessarily positive due to the additional volume increase at oblique particle incidence. Then, expanding the deterministic part on the right-hand side (RHS) of Eq. (10) up to the order $\mathcal{O}(\vec{\nabla}^3, (\vec{\nabla} H)^2)$ and neglecting all corrections to the deposition noise yields

$$\partial_t H = a_1 \vec{\nabla}^2 H + a_2 \vec{\nabla}^4 H + a_3 \vec{\nabla}^2 (\vec{\nabla} H)^2 + a_4 (\vec{\nabla} H)^2 + a_5 M + F + \eta. \quad (11)$$

Finally, using the transformation $h(\vec{x},t) = H(\vec{x},t) - Ft$ with $h(\vec{x},t)$ being the surface profile in the comoving frame, one obtains the stochastic growth equation

$$\partial_t h = a_1 \vec{\nabla}^2 h + a_2 \vec{\nabla}^4 h + a_3 \vec{\nabla}^2 (\vec{\nabla} h)^2 + a_4 (\vec{\nabla} h)^2 + a_5 M + \eta. \quad (12)$$

The first and the fifth term on the RHS of Eq. (12) are related to the deflection of the initially perpendicular incident particles caused by interatomic attraction. When the particles are close to the surface their trajectories are bent towards the surface. As a consequence, more particles arrive at places with $\vec{\nabla}^2 h < 0$ than at places with $\vec{\nabla}^2 h > 0$ [16]. In a simplified model, this deflection (in a direction perpendicular to the surface) happens instantaneously when a particle arrives at a distance b from the surface, as shown in the upper part of Fig. 2. b characterizes the typical range of the interatomic force. A detailed mathematical analysis of this simplified model yields the explicit relations $a_1 = -Fb$ and $a_5 = Fb^2$ [12]. Since b is very small (typically of the order 10^{-1} nm) compared to the radius of the surface curvature the term proportional to a_5 in Eq. (12) can safely be neglected. On the other hand, the negative coefficient a_1 represents the growth instability that results in the experimentally observed mound-like surface structure on vapor deposited amorphous films [7–11].

The second term on the RHS of Eq. (12) represents the surface diffusion suggested by Mullins [17]. The particles arrive at the surface, diffuse there and relax at surface sites that offer a sufficiently strong binding. Because these binding places are more frequent on surface areas with positive curvature $\vec{\nabla}^2 h$, the surface diffusion results in a current of the form $\vec{j} \sim \vec{\nabla} (\vec{\nabla}^2 h)$, as shown in the middle part of Fig. 2. This surface current adds the term $-\vec{\nabla} \cdot \vec{j} \sim -\vec{\nabla}^4 h$ to the growth equation. Therefore, the sign of a_2 is negative. Rost [18] has recently suggested the explicit expression $a_2 = -2l^2 \ln(l/a) F(\Omega \gamma / \epsilon_0)$ where l denotes the diffusion length of

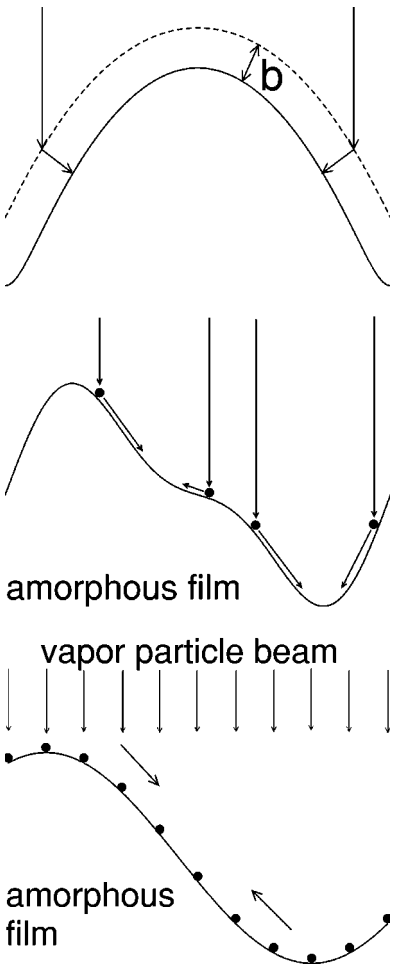

FIG. 2. Microscopic effects of amorphous thin film growth. Upper part: Deflection of particles due to interatomic forces. Middle part: Surface diffusion of deposited particles to places with larger curvature. Lower part: Equilibration of the inhomogeneous particle concentration due to the geometry of the surface.

the particles, a the average distance of the potential minima seen by the diffusing particles, Ω the atomic volume, γ the surface tension, and ϵ_0 the width of the distribution of the depths of the potential wells.

The third term on the RHS of Eq. (12) is related to the equilibration of the inhomogeneous concentration of the diffusing particles on the surface, as suggested in [3,19]. If only the just deposited particles diffuse before their relaxation, their surface concentration is weighted by the surface inclination, $n \sim 1/\sqrt{1+(\vec{\nabla}h)^2} \approx 1-(\vec{\nabla}h)^2/2$ [19], as shown in the lower part of Fig. 2. This causes a diffusion current of the type $\vec{j} \sim -\vec{\nabla}n \sim \vec{\nabla}(\vec{\nabla}h)^2$ and leads to the $a_3\vec{\nabla}^2(\vec{\nabla}h)^2$ term with $a_3<0$. A detailed discussion of the concentration equilibration [12] yields the explicit relation $a_3=-Fl^2/8$ where l^2 represents the mean square of the diffusion length of the particles.

The term proportional to a_4 is related to the aforementioned density variations. It is the only term in the deterministic part of the RHS of Eq. (12) that cannot be written in the form $-\vec{\nabla}\cdot\vec{j}$. Therefore, it leads to a nonzero excess velocity, i.e., there is a nonlinear relation between the mean layer thickness $\langle H\rangle(t)=\langle(1/L^2)\int d^2x H(\vec{x},t)\rangle$ and time

$$\langle H\rangle(t)=Ft+\int_0^t dt'\left\langle \frac{1}{L^2}\int d^2x a_4(\vec{\nabla}H)^2\Big|_{\vec{x},t'}\right\rangle. \quad (13)$$

By neglecting the term proportional to a_5 we obtain the *minimal* deposition equation for amorphous thin film growth in the presence of significant density variations [12,13]

$$\partial_t h=a_1\vec{\nabla}^2h+a_2\vec{\nabla}^4h+a_3\vec{\nabla}^2(\vec{\nabla}h)^2+a_4(\vec{\nabla}h)^2+\eta, \quad (14)$$

with a_1, a_2, a_3 being negative and a_4 being positive.

A comparison with experimental data for amorphous $Zr_{65}Al_{7.5}Cu_{27.5}$ film growth [14] has recently shown a good quantitative agreement between this model equation (14) and the experiment for a layer thickness up to 480 nm. For this specific system at room temperature, the coefficients entering in Eq. (14) at a deposition rate of $F=0.79$ nm/s have been identified as [14]

$$a_1=-0.0826\ \text{nm}^2/\text{s},\quad a_2=-0.319\ \text{nm}^4/\text{s},$$
$$a_3=-0.10\ \text{nm}^3/\text{s},\quad a_4=0.055\ \text{nm/s}, \quad (15)$$
$$D=0.0174\ \text{nm}^4/\text{s}.$$

Using the relations $a_1=-Fb$, $a_2=-2l^2\ln(l/a)F(\Omega\gamma/\epsilon_0)$, $a_3=-Fl^2/8$, $[\rho(\vec{\nabla}h)]^{-1}=\rho_0^{-1}[1+(a_4/F)(\vec{\nabla}h)^2]$, and $2D=F\Omega$ [12], one can infer that every coefficient given in Eq. (15) has a realistic order. Therefore, Eq. (14) constitutes a reliable theoretical model for amorphous thin film growth, at least for the considered range of the layer thickness.

III. RESULTS

A. Comparison with experimental results

In this section, we carry on our comparison [14] with the experimental results on the surface morphology of amorphous $Zr_{65}Al_{7.5}Cu_{27.5}$ films prepared by electron beam evaporation [7–10]. The correlation length $R_c(t)$ and the surface roughness $w(t)$ are determined by the experimentally accessible height-height correlation function

$$C(r,t)=\left\langle\left\langle \frac{1}{L^2}\int d^2x[h(\vec{x},t)-\overline{h}(t)][h(\vec{x}+\vec{r},t)-\overline{h}(t)]\right\rangle\right\rangle_{|\vec{r}|=r}, \quad (16)$$

where $\overline{h}(t)=(1/L^2)\int d^2x h(\vec{x},t)$ denotes the spatially average of the height, and $\langle\langle\cdots\rangle\rangle_{|\vec{r}|=r}$ denotes a combined ensemble and radial average. Specifically, $R_c(t)$ is given by the first maximum of $C(r,t)$ occuring at nonzero values of r and the square of the surface roughness results from taking the limit $r=0$ in $C(r,t)$, i.e., $w^2(t)=C(0,t)$. The quantities $w(t)$ and $R_c(t)$ characterize the typical height and periodicity length

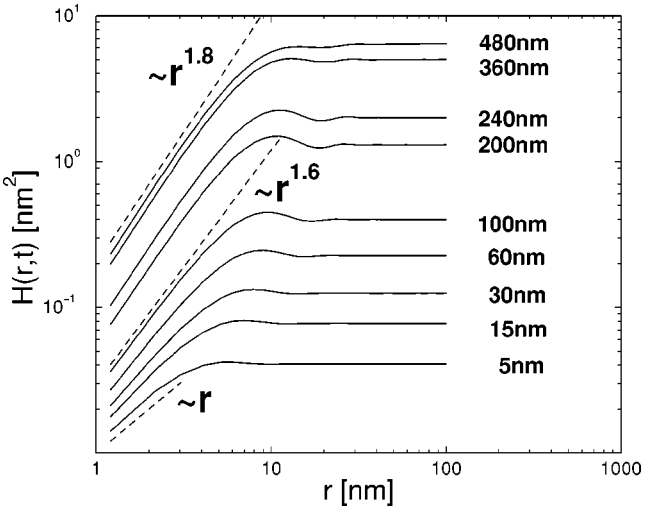

FIG. 3. Height-difference correlation function $H(r,t)$ for various values of Ft calculated from the nonlinear stochastic growth equation (14) on an interval $[0,L]^2$ of the length $L=200$ nm subject to periodic boundary conditions. The parameters are given in Eq. (15). For reference, the dashed lines indicate the different power-law behaviors.

scales of the surface structure. Another related quantity is the height-difference correlation function

$$H(r,t)=\left\langle \left\langle \frac{1}{L^2}\int d^2x[h(\vec{x},t)-h(\vec{x}+\vec{r},t)]^2 \right\rangle \right\rangle_{|\vec{r}|=r}. \tag{17}$$

Since the relation

$$H(r,t)=2w^2(t)-2C(r,t) \tag{18}$$

holds, it connects the two different correlation functions and, moreover $H(r,t)\to 2w^2(t)$ results in the limit of large radii $r\to\infty$.

In the afore-mentioned comparison with experimental results [14], a quantitative agreement of $R_c(t)$ and $w(t)$ between the model equation (14) and the experimental data has been achieved up to a layer thickness of 480 nm by using the coefficients given in Eq. (15). Here, we extend this investigation by comparing theoretical data on $H(r,t)$ obtained by numerical simulations of Eq. (14) with the coefficients (15) using the method explained in Appendix C of [12] and corresponding experimental data [7,9,10]. The height-difference correlation function $H(r,t)$ resulting from Eq. (14) for various values of Ft is shown in Fig. 3. Note that, despite the presence of a nonzero excess velocity, the difference between the mean layer thickness $\langle H\rangle$ and Ft is less than 1.1% even for the largest layer thickness. Therefore, the different values of Ft in Fig. 3 represent the mean film thickness $\langle H\rangle$ in first approximation. We obtain a good quantitative agreement with the experimentally observed height-difference correlation function $H(r,t)$ on amorphous $Zr_{65}Al_{7.5}Cu_{27.5}$ films (cf. Fig. 6 in [7], Fig. 3 in [9], and Fig. 5 in [10]). For large radii, this agreement is a result of the coincidence of the surface roughnesses $w(t)$ since $H(r,t)$ saturates at $2w^2(t)$ for $r\to\infty$. More interesting is the behavior of $H(r,t)$ for small radii r. From the numerical results in Fig. 3 one can infer that the increase of $H(r,t)$ follows a power-law behavior

$$H(r,t)\sim r^{\kappa(\langle H\rangle)}, \tag{19}$$

where the exponent κ explicitly depends on the layer thickness and increases *monotonically* from $\kappa=1$ for $\langle H\rangle \approx 5$ nm up to $\kappa=1.8$ for $\langle H\rangle\approx 480$ nm. A similar behavior can also be read off from the experimental results in Ref. [9,10] where the corresponding exponent κ varies from $\kappa=1.4$ for $\langle H\rangle\approx 100$ nm to $\kappa=1.6$ for $\langle H\rangle\approx 480$ nm. Moreover, also the nonmonotonic crossover of $H(r,t)$ to a saturation for large r in form of a local maximum and a subsequent minimum (over and undershooting) coincides with the experimental finding [9,10]. $C(r,t)$ possesses a first maximum at $r=R_c(t)$. Therefore, using Eq. (18), the position of the first local minimum of $H(r,t)$ is determined by the correlation length $R_c(t)$. From the experimental data for $Zr_{65}Al_{7.5}Cu_{27.5}$ films obtained by scanning tunneling microscopy, also direct visualizations of the surface morphology of individual samples at different stages of growth processes have been obtained [8–10], cf. also the right row in Fig. 4. For comparison, the surface morphology resulting from a numerical integration of Eq. (14) with the coefficients (15) for *one individual* growth process starting from a flat substrate $h(\vec{x},0)=0$ is shown in the left row of Fig. 4. Obviously, the visual comparison of the evolution of the surface structures between theory and experiment shows a striking similarity. In particular, the evolution of the moundlike structures and their typical length scale are caused by the competition between the growth instability $a_1\vec{\nabla}^2 h$ and the surface diffusion represented by the $a_2\vec{\nabla}^4 h$ term. Only for the largest layer thickness 480 nm the calculated surface morphology is a little bit coarser than the experimentally observed structure despite the coincidence of the correlation length $R_c(t)$ [14].

B. Effects of density inhomogeneities at larger film thicknesses

The good agreement between numerical simulations of Eq. (14) and the available experimental data on $Zr_{65}Al_{7.5}Cu_{27.5}$ films for a layer thickness up to 480 nm raises the question whether the growth process has already reached the asymptotic time evolution or not. In order to investigate this point in detail, we perform numerical simulations of the nonlinear stochastic growth equation (14) up to a layer thickness of approximately 5000 nm. We also discuss the impact of both nonlinear terms in Eq. (14).

The solid lines in Fig. 5 correspond to the resulting correlation length $R_c(t)$ and surface roughness $w(t)$ using the coefficients given in Eq. (15). As a general consequence, the nonlinear terms lead to a drastic slow down of the increase of the surface roughness $w(t)$ above the largest experimentally observed film thickness $\langle H\rangle=480$ nm. We find a growth behavior of the surface roughness given by $w(t)\sim t^{0.045}$ in the thickness interval 480 nm$\leqslant\langle H\rangle\leqslant$5000 nm. For small layer thicknesses $\langle H\rangle\leqslant 240$ nm the linear parts of Eq. (14) dominate the growth behavior and result in an exponential growth of $w(t)$ due to the presence of a linear instability

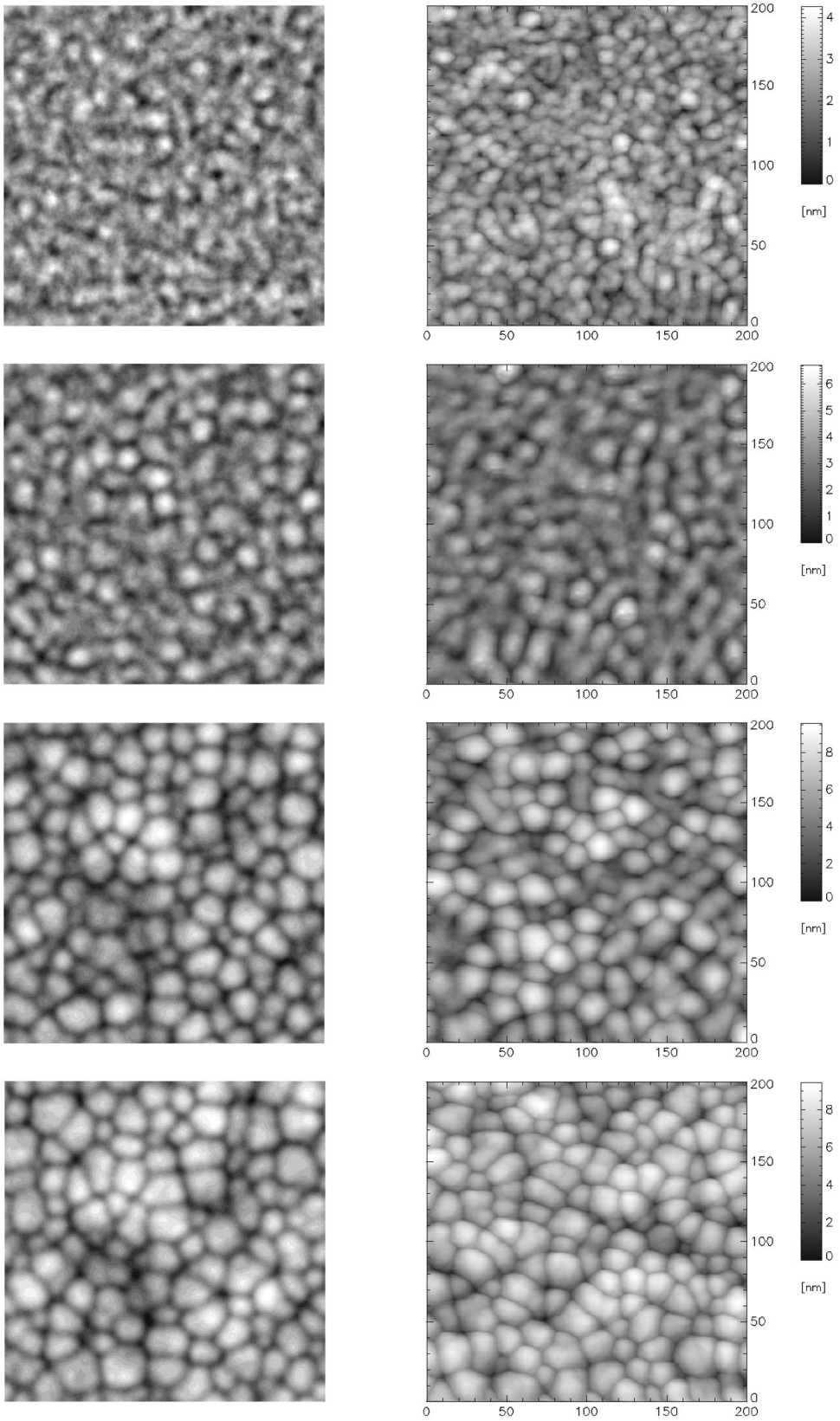

FIG. 4. Left row: Surface morphologies for $Ft=100$ nm, 200 nm, 360 nm, 480 nm (from top to bottom) calculated from Eq. (14) on an interval $[0,L]^2$ of the size $L=200$ nm subject to periodic boundary conditions. The parameters are given in Eq. (15). Right row: Experimentally recorded surface morphologies of vapor deposited amorphous $Zr_{65}Al_{7.5}Cu_{27.5}$ films of $\langle H\rangle=100$ nm, 200 nm, 360 nm, 480 nm thickness (from top to bottom), taken from [8–10]. The maxima (minima) of the height profiles $h(\vec{x},t)$ are marked in white (black).

[14]. The correlation length $R_c(t)$ possesses a maximum at $\langle H\rangle\approx 360$ nm followed by an initially strong decrease until it saturates in a very slow decrease for layer thicknesses $\langle H\rangle\geqslant 600$ nm. At these later stages the value of the correlation length $R_c(t)$ lies in the range of the wavelength of the most unstable mode $2\pi\sqrt{2a_2/a_1}=17.5$ nm. By setting $a_3=0$ we observe that the slow down of the increase of $w(t)$ occurs at a larger value of $w(t)$, see the dashed line in Fig. 5.

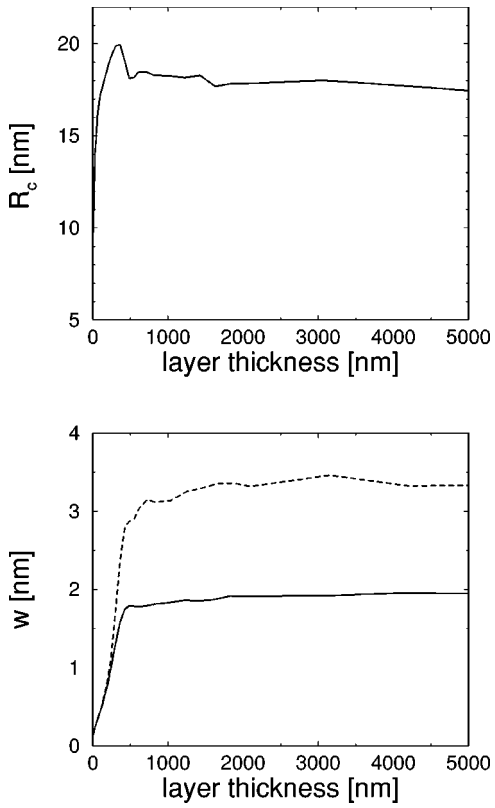

FIG. 5. Correlation length R_c and surface roughness w as functions of the layer thickness calculated from the nonlinear growth equation (14) using the parameters given in Eq. (15) (solid lines). To demonstrate the significant influence of the nonlinear growth term $\propto\vec{\nabla}^2(\vec{\nabla}h)^2$, we show for comparison the surface roughness w that results by setting $a_3=0$ (dashed line).

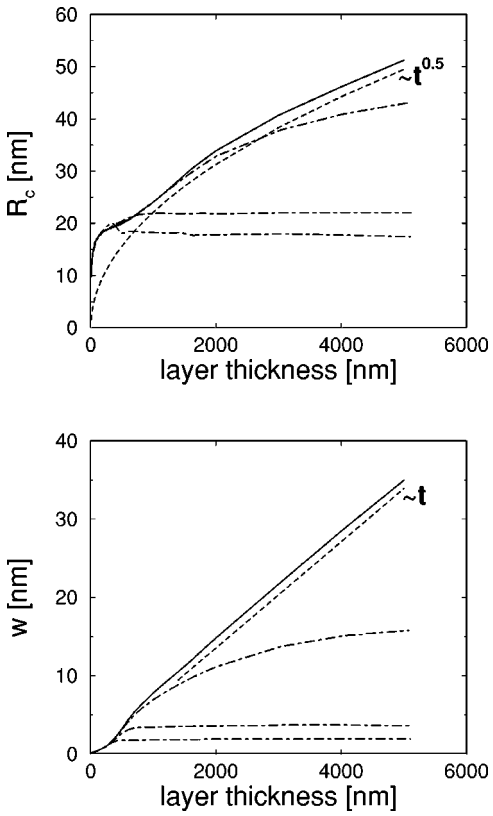

FIG. 6. Correlation length R_c and surface roughness w as functions of the layer thickness calculated from the nonlinear growth equation (4) without the inclusion of the $a_4(\vec{\nabla}h)^2$ term (solid lines). To demonstrate the significant influence of the nonlinear term $(\vec{\nabla}h)^2$, we show for comparison the prediction that results from Eq. (14) using various values of $a_4=0.0016$ nm/s, 0.016 nm/s, and 0.055 nm/s (dash-dotted lines, from top to bottom). All other parameters are as given in Eq. (15). The dashed lines are calculated from $R_c\sim\sqrt{t}$ and $w\sim t$.

In this case, the growth behavior of $w(t)$ at large film thicknesses 480 nm$\leqslant\langle H\rangle\leqslant$5000 nm is given by $w(t)\sim t^{0.06}$. In addition, we note that the correlation length $R_c(t)$ now ceases to exist above $\langle H\rangle\approx 300$ nm (not shown), because the first maximum of the height-height correlation function $C(r,t)$ vanishes.

To demonstrate the important impact of the term $a_4(\vec{\nabla}h)^2$ that represents the potential density variations on the evolution of the surface structure we present, for comparison, results by setting $a_4=0$, given by the solid lines in Fig. 6. In this case, we obtain a linear increase of the surface roughness $w(t)\sim t$ and an algebraic growth law $R_c(t)\sim\sqrt{t}$ for the correlation length [12]. This behavior can be attributed to a coarsening of the moundlike surface structure, that ends in a final state with only *one* mound on any finite interval $[0,L]^2$ subject to periodic bounding conditions [12]. Figure 6 also shows the correlation length $R_c(t)$ and roughness $w(t)$ that result from Eq. (14) using various different values of the coefficient a_4, while the other parameters are kept at their values given in Eq. (15). As a general result, we observe that decreasing a_4 increases the values of $R_c(t)$ and $w(t)$ at large layer thicknesses. At the smallest nonzero a_4, $a_4=0.0016$ nm/s, a saturation of $R_c(t)$ and $w(t)$ has not yet happened at the end of the simulation.

The height-difference correlation function $H(r,t)$ resulting from Eq. (14) including the nonlinear term $a_4(\vec{\nabla}h)^2$ is shown in Fig. 7 and exhibits a saturation at small radii r,

$$H(r,t)\sim r^{1.8}. \tag{20}$$

The increase of $H(r,t)$ with time at large radii corresponds to the very slow increase of the surface roughness $w(t)$ above a film thickness of $\langle H\rangle\approx 480$ nm as shown in Fig. 5.

In Fig. 8 the different evolutions of the surface morphologies with and without the impact of the density inhomogeneities are compared by visualizing the images of the height profiles being calculated from Eqs. (14) and (4). Again, the coefficients given in Eq. (15) were used. Setting a_4 equals zero the moundlike surface structure coarsens with time and develops into a final state (not shown) that possesses only one mound on the interval $[0,L]^2$ [12]. Moreover, the height profile at $Ft=480$ nm now looks rather different from its experimentally observed counterpart that is shown in Fig. 4. For nonzero a_4 the surface morphology becomes stationary above a film thickness of approximately 480 nm at a typical mound size that is independent from the size L of the interval

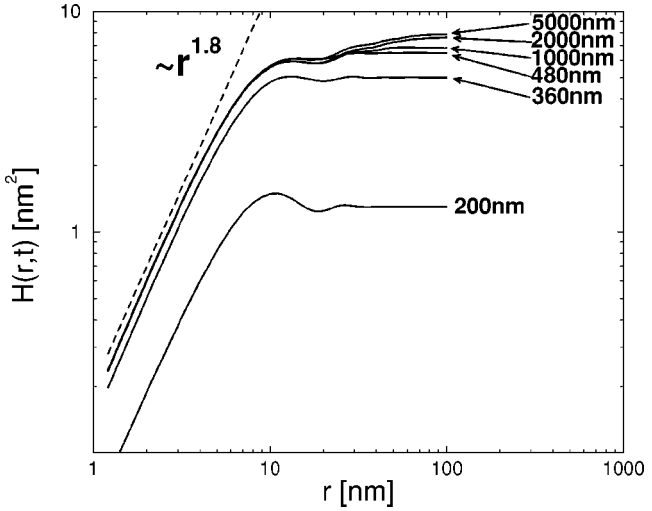

FIG. 7. Height-difference correlation function $H(r,t)$ for various values of Ft calculated from the nonlinear stochastic growth equation (14) on an interval $[0,L]^2$ of the length $L=200$ nm subject to periodic boundary conditions. The parameters are given in Eq. (15).

$[0,L]^2$ and is basically given by the critical wavelength $2\pi\sqrt{2a_2/a_1}$. Yet the spatial distribution of individual mounds and valleys is always in change. The latter is *not* a consequence of the deposition noise η. Similar to the related Kuramoto-Sivashinsky equation, $\partial_t h = a_1\vec{\nabla}^2 h + a_2\vec{\nabla}^4 h + a_4(\vec{\nabla}h)^2$, the irregular change of the moundlike surface structure results from the nonlinear term $a_4(\vec{\nabla}h)^2$ [20]. If Eq. (14) is applied small mounds vanish and large mounds grow at the expense of their smaller neighbors, until they split into smaller mounds. On the other hand, in the absence of the term proportional to a_4 the large mounds do not split.

To estimate the impact of the deposition noise η, we integrated Eq. (14) using the parameters given in Eq. (15), but we "switched off" the noise term η at $Ft=100$ nm. We obtained the same irregularly changing moundlike surface structure. As only significant difference, the mounds then look smoother on a smaller length scale. The differences in the behavior of $R_c(t)$, $w(t)$, and $H(r,t)$ are only quantitative, but not qualitative: the surface roughness $w(t)$ is about 7% smaller and the correlation length $R_c(t)$ is about 5% larger than in the stochastic case at layer thicknesses $\langle H\rangle \geqslant 800$ nm. The small influence of the deposition noise is not too surprising due to the smallness of the coupling constant $g=4Da_4^2/a_1^3=-0.378$, that results from the parameters given in Eq. (15).

Next, we investigate the size of the density variations resulting from Eqs. (14) and (15) and their temporal evolutions. On an inclined surface area the local density is decreased by

$$\rho(\vec{\nabla}h)=\rho_0/\gamma \quad \text{with} \quad \gamma=1+(a_4/F)(\vec{\nabla}h)^2, \qquad (21)$$

where a_4/F is in the range of about 0.07 if the experimentally determined parameters $F=0.79$ nm/s and a_4

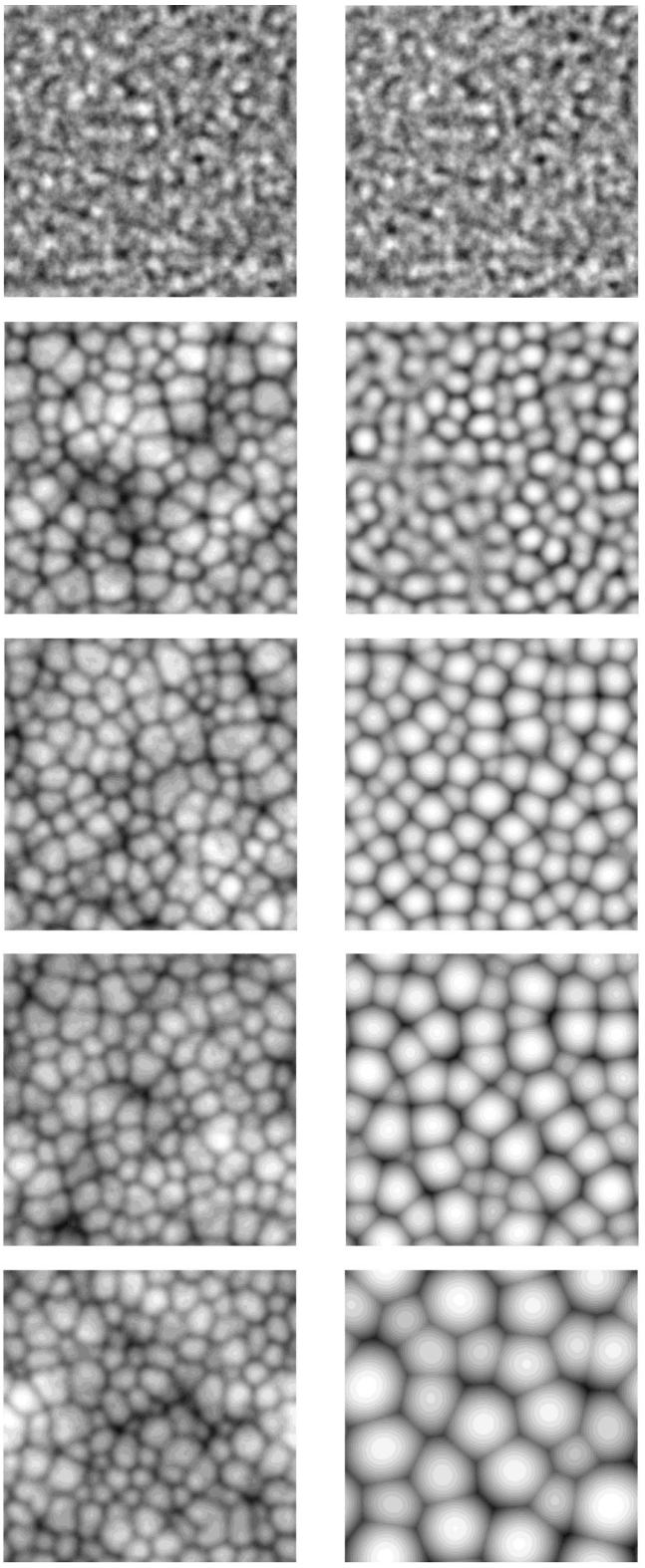

FIG. 8. Surface morphologies for $Ft=100$ nm, 480 nm, 1000 nm, 2000 nm, and 5000 nm (from top to bottom) calculated from Eq. (14) (left row) and Eq. (4) (right row) on an interval $[0,L]^2$ of the size $L=200$ nm subject to periodic boundary conditions. The parameters are given in Eq. (15). The maxima (minima) of the height profiles $h(\vec{x},t)$ are marked in white (black).

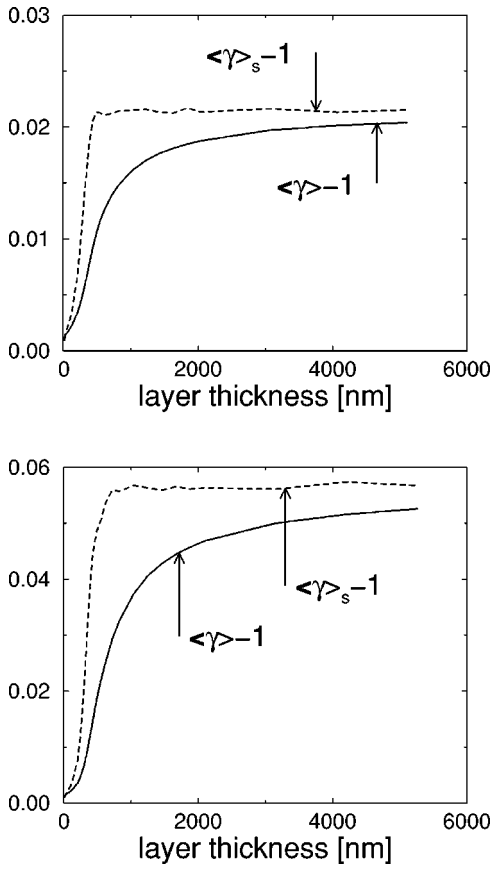

FIG. 9. Upper part: Density reduction $\gamma-1=(a_4/F)(\vec{\nabla}h)^2$ calculated from Eq. (14) averaged over the surface (dashed line) and averaged over the entire film (solid line). The coefficients are given in Eq. (15). Lower part: Density reduction $\gamma-1=(a_4/F)(\vec{\nabla}h)^2$ that results from Eq. (14) by setting $a_3=0$, averaged over the surface (dashed line) and averaged over the entire film (solid line). All other coefficients are as given in Eq. (15).

$=0.055$ nm/s are used. In Fig. 9 we show the density reduction averaged over the surface

$$\langle\gamma\rangle_s-1=\left\langle(1/L^2)\int d^2x(a_4/F)(\vec{\nabla}h)^2\right\rangle \tag{22}$$

and averaged over the entire film

$$\langle\gamma\rangle-1=\langle H\rangle/(Ft)-1, \tag{23}$$

that result from Eq. (14) with and without the inclusion of the other nonlinearity $a_3\vec{\nabla}^2(\vec{\nabla}h)^2$. Similar to the roughness $w(t)$ the density reduction $\langle\gamma\rangle_s-1$ first rapidly increases and then remains constant in the interval 700 nm$\leqslant\langle H\rangle\leqslant$5000 nm. This also leads to a slow down of the increase of $\langle\gamma\rangle-1$ since the evolution of $\langle\gamma\rangle-1$ is delayed in comparison with the evolution of $\langle\gamma\rangle_s-1$. The nonlinear term $a_3\vec{\nabla}^2(\vec{\nabla}h)^2$ lessens the density reduction. We also find that the standard deviation of γ on the surface $(\langle[\gamma-\langle\gamma\rangle_s]^2\rangle_s)^{1/2}$ first increases and later, at film thicknesses 480 nm$\leqslant\langle H\rangle\leqslant$5000 nm, reaches a constant value of 0.017 with and 0.047 without the inclusion of the term proportional to a_3.

Finally we ascertain that even for the smallest nonzero value of a_4 that was applied in this study, $a_4=0.0016$ nm/s (see Fig. 6), a saturation of the surface morphology will occur. Therefore, we numerically solved Eq. (14) using this value of a_4 and the other parameters given in Eq. (15) on an interval $[0,L]^2$ of the size $L=400$ nm subject to periodic boundary conditions. In order to accelerate the calculation we now "switched off" the deposition noise η at $Ft=100$ nm. We obtained a drastic slow down of the increase of the roughness $w(t)$ and the correlation length $R_c(t)$ at very large layer thicknesses 20 000 nm$\leqslant\langle H\rangle\leqslant$120 000 nm (not shown). Hence the smallness of a_4 results in a delay of the saturation of the moundlike surface morphology. In addition, we note that at these later stages the correlation length (and typical mound size) $R_c(t)$ is in the range of $R_c(t)\approx46$ nm and is therefore larger than the critical wavelength $2\pi\sqrt{2a_2/a_1}=17.5$ nm.

C. Discussion

The numerical simulations of Eq. (14) using the experimentally determined parameters given in Eq. (15) indicate that the nonlinear term $a_4(\vec{\nabla}h)^2$ basically leads to a saturation of the surface structure, at least within the investigated range of time. The surface morphology consists of mounds that change irregularly in time and space. Their typical size, however, is given by the wavelength of the most unstable mode $2\pi\sqrt{2a_2/a_1}$ if a_4 is not too small. It might be possible that the surface still roughens on length scales larger than the mound size, as in the case of the Kuramoto-Sivashinsky equation [20].

It has not been rigorously proven yet that a saturation of the typical mound size occurs for *any* positive value a_4. However, this seems reasonable since at large length scales the term $a_4(\vec{\nabla}h)^2$ becomes much larger in comparison to the other nonlinearity $a_3\vec{\nabla}^2(\vec{\nabla}h)^2$ which is responsible for the coarsening process (see the right row in Fig. 8). If a_4 is small, the nonlinear term $a_4(\vec{\nabla}h)^2$ does not become relevant before a coarsening of the moundlike surface morphology has occured. This explains why the surface structure saturates at later stages and larger length scales if a_4 is small. The growth behavior of the solutions of Eq. (14) depends basically on the dimensionless constant $\nu=(a_2a_4)/(a_1a_3)$.

The previous considerations hold in the physically relevant case, i.e., a_1 and a_2 are negative and a_3 and a_4 have opposite signs. On the other hand, if a_3 and a_4 had the same signs, the two nonlinear terms in Eq. (14) would compensate each other at the wavelength $2\pi\sqrt{a_3/a_4}$. If, additionally, the absolute value of a_4 was small enough, this wavelength would be larger than $2\pi\sqrt{a_2/a_1}$ and would therefore belong to an unstable mode. Then, the surface roughness $w(t)$ would increase at least exponentially.

IV. CONCLUSIONS

In this study, we have presented a nonlinear stochastic field equation (14) for amorphous film growth that can serve

as a minimal model if the possibility of density inhomogeneities is taken into account. Starting from the condition of no particle desorption, using the symmetries relevant for amorphous film growth and allowing for density variations depending on the surface slope we derived the simplest functional form of an equation capable for describing the growth of amorphous films. A detailed comparison of available experimental data with the numerical simulations of the statistical measures of the surface morphology, $R_c(t)$, $w(t)$, and the height-difference correlation function $H(r,t)$ and also with direct visualizations of the surface evolution reveals a very good agreement in the considered range of the layer thickness. For the not yet experimentally explored range of layer thicknesses $\langle H\rangle \geqslant 480$ nm, we gave detailed predictions for the expected surface morphology on the basis of Eqs. (14) and (15). Most remarkably, the suggested density variations that are represented by a nonlinear term proportional to $(\vec{\nabla} h)^2$ in Eq. (14) stabilize the surface morphology to a typical moundlike structure. We hope that our study motivates further experimental studies on amorphous film growth.

ACKNOWLEDGMENTS

This work has been supported by the DFG-Sonderforschungsbereich 438 München/Augsburg, TP A1. We also thank S. G. Mayr, M. Moske, and K. Samwer for insightful discussions and providing files of previously published data.

APPENDIX: AMORPHOUS SURFACE GROWTH: THE ROLE OF THE GRINFELD INSTABILITY

As experiments [19] show, the growth of vapor deposited amorphous transition metal alloy films is accompanied with the occurrence of lateral stresses of the order $p \approx 1$ GPa. This poses the question if the formation of the experimentally observed moundlike surface structure on the amorphous films can be the result of an elastic instability, namely the Grinfeld instability [21–23,18]. Here, we show that this possibility is not taking place by comparing the decrease of the elastic energy and the increase of the surface energy that are caused by the occurrence of the moundlike surface structure at the observed wavelength.

Amorphous films grow under lateral stresses, implying in first approximation that the corresponding stress tensor σ_{ik} possesses only two nonzero components $\sigma_{xx}=\sigma_{yy}=p$. If the amorphous film has an uneven surface, however, this stress tensor σ_{ik} does not fulfill the boundary conditions on the surface and needs to be supplemented by a correction τ_{ik}. Then, the boundary conditions on the surface are determined by

$$(\sigma_{ik}+\tau_{ik})n_k=\gamma\vec{\nabla}\cdot\left(\frac{\vec{\nabla} h}{\sqrt{1+(\nabla h)^2}}\right)n_i \qquad \text{(A1)}$$

for $i=1,2,3$, where

$$\vec{n}=\frac{1}{\sqrt{1+(\nabla h)^2}}\begin{pmatrix}-\vec{\nabla} h\\ 1\end{pmatrix} \qquad \text{(A2)}$$

denotes the unit vector perpendicular to the surface and the RHS of Eq. (A1) represents the surface tension. The correction τ_{ik} depends in lowest order linearly on the gradient $\vec{\nabla} h$. If only such terms in Eq. (A1) that are linear in $\vec{\nabla} h$ are taken into consideration one obtains the simplified boundary conditions

$$-p\frac{\partial h}{\partial x}+\tau_{xz}=0 \quad \text{for} \quad i=x, \qquad \text{(A3)}$$

$$-p\frac{\partial h}{\partial y}+\tau_{yz}=0 \quad \text{for} \quad i=y, \qquad \text{(A4)}$$

$$\tau_{zz}=\gamma\vec{\nabla}^2 h \quad \text{for} \quad i=z. \qquad \text{(A5)}$$

If the viscosity of the amorphous material is not too large, the additional stress field τ_{ik} leads to motion inside the film. Due to energy dissipation these motions quickly fade away to a state where the mechanical stresses compensate each other. Therefore, the additional stress field τ_{ik} fulfills the conditions

$$\frac{\partial \tau_{ik}}{\partial x_k}=0 \quad i=1,2,3 \qquad \text{(A6)}$$

inside the film and follows quasistatically the alterations of the height profile $h(\vec{x},t)$.

The additional stress field τ_{ik} is related to an additional deformation u_i by Hooke's law

$$\tau_{ik}=Ku_{ll}\delta_{ik}+2\mu\left(u_{ik}-\frac{1}{3}u_{ll}\delta_{ik}\right), \qquad \text{(A7)}$$

where the strain tensor u_{ik} is defined by

$$u_{ik}=\frac{1}{2}\left(\frac{\partial u_i}{\partial x_k}+\frac{\partial u_k}{\partial x_i}\right). \qquad \text{(A8)}$$

Since the interface between the film and the substrate is even, the components τ_{xz}, τ_{yz}, τ_{zz}, u_x, u_y, and u_z are continuous functions on this interface.

By using the boundary conditions on the surface (A3)–(A5) and on the film-substrate interface and the Eqs. (A6)–(A8), one can determine the deformation u_i and the stress field τ_{ik} inside the film [24]. To simplify the calculation we assume that the elastic moduli K and μ have the same values in the film and in the substrate [18]. Note that the surface morphologies on vapor deposited $Zr_{65}Al_{7.5}Cu_{27.5}$ films were found to be independent from the details of the substrate, even if the substrate consisted of a relaxed $Zr_{65}Al_{7.5}Cu_{27.5}$ film (prepared at higher temperature) [8,19].

Since Eqs. (A3)–(A8) are linear they can be solved by a Fourier transformation in the x and y coordinates

$$\tilde{\tau}_{ik}(k_x,k_y,z,t)=\int_0^L dx\int_0^L dy\,\tau_{ik}(x,y,z,t)\exp[-i(k_x x+k_y y)], \tag{A9}$$

$\tilde{u}_i(k_x,k_y,z,t)$ and $\tilde{u}_{ik}(k_x,k_y,z,t)$ are given by analogous definitions. Next, we put the x axis in the direction of the wave vector $\vec{k}=(k_x,k_y)$, yielding $k_x=k$ and $k_y=0$. Then, the resulting deformation in Fourier space is given by $\tilde{u}_y=0$ and

$$\begin{pmatrix}\tilde{u}_x\\ \tilde{u}_z\end{pmatrix}=\frac{p}{2\mu}\begin{pmatrix} i\dfrac{K+4\mu/3}{K+\mu/3}+ikz\\ -\dfrac{\mu}{K+\mu/3}+kz\end{pmatrix}\tilde{h}e^{kz}+\frac{\gamma k}{2\mu}\begin{pmatrix} i\dfrac{\mu}{K+\mu/3}+ikz\\ -\dfrac{K+4\mu/3}{K+\mu/3}+kz\end{pmatrix}\tilde{h}e^{kz}. \tag{A10}$$

Using Eq. (A8) we obtain the strain tensor

$$\tilde{u}_{xx}=-\frac{p}{2\mu}\left(\frac{K+4\mu/3}{K+\mu/3}+kz\right)k\tilde{h}e^{kz}-\frac{\gamma k}{2\mu}\left(\frac{\mu}{K+\mu/3}+kz\right)k\tilde{h}e^{kz}, \tag{A11}$$

$$\tilde{u}_{zz}=\frac{p}{2\mu}\left(\frac{K-2\mu/3}{K+\mu/3}+kz\right)k\tilde{h}e^{kz}+\frac{\gamma k}{2\mu}\left(-\frac{\mu}{K+\mu/3}+kz\right)k\tilde{h}e^{kz}, \tag{A12}$$

$$\tilde{u}_{xz}=\frac{ip}{2\mu}(1+kz)k\tilde{h}e^{kz}+\frac{i\gamma k}{2\mu}k^2z\tilde{h}e^{kz}, \tag{A13}$$

$$\tilde{u}_{yy}=\tilde{u}_{xy}=\tilde{u}_{yz}=0. \tag{A14}$$

Finally, Eq. (A7) yields the additional stress field

$$\tilde{\tau}_{xx}=-p(2+kz)k\tilde{h}e^{kz}-\gamma k(1+kz)k\tilde{h}e^{kz}, \tag{A15}$$

$$\tilde{\tau}_{yy}=-(p+\gamma k)\frac{K-2\mu/3}{K+\mu/3}k\tilde{h}e^{kz}, \tag{A16}$$

$$\tilde{\tau}_{zz}=pk^2z\tilde{h}e^{kz}+\gamma k(-1+kz)k\tilde{h}e^{kz}, \tag{A17}$$

$$\tilde{\tau}_{xz}=ip(1+kz)k\tilde{h}e^{kz}+i\gamma k^3z\tilde{h}e^{kz}, \tag{A18}$$

$$\tilde{\tau}_{xy}=\tilde{\tau}_{yz}=0. \tag{A19}$$

One can verify that this stress tensor fulfills the Eqs. (A3)–(A6) in Fourier space. Note that in this calculation the origin of the z axis ($z=0$) coincides with the mean surface height.

The additional stress and strain fields τ_{ik} and u_{ik} result in an additional elastic energy per volume, $\sigma_{ik}u_{ik}+\tau_{ik}u_{ik}/2$. Insertion of the solutions given in Eqs. (A11)–(A19) and integration over the film yields the change of the elastic energy, that is caused by the height variations $h(\vec{x},t)$ on an interval $[0,L]^2$ subject to periodic boundary conditions [24]

$$E_{el}(t)=\frac{1}{L^2}\sum_{\vec{k}}\left[-E\frac{1+\sigma}{1-\sigma}\alpha^2k+\frac{\gamma^2k^3}{E}(1-\sigma^2)\right]|\tilde{h}(\vec{k},t)|^2. \tag{A20}$$

Here, $\tilde{h}(\vec{k},t)=\int d^2x h(\vec{x},t)\exp(-i\vec{k}\cdot\vec{x})$ denotes the height profile in Fourier space, E denotes Young's modulus, $\sigma\in[0,1/2]$ the Poisson number, $\alpha=u^0_{xx}=u^0_{yy}=(1-\sigma)p/E$ the lateral deformation in the case of an even surface, γ the surface tension, and $k=|\vec{k}|=2\pi/\lambda$ the wave number. The negative term on the RHS of Eq. (A20) is caused by the lateral stress p and represents the Grinfeld instability.

On the other hand, an uneven surface results in an increase of the surface energy

$$E_{sf}(t)=\frac{1}{L^2}\sum_{\vec{k}}\frac{1}{2}\gamma k^2|\tilde{h}(\vec{k},t)|^2. \tag{A21}$$

The addition of elastic energy and surface energy yields the total change of the free energy of the film resulting from the occurrence of an uneven surface profile on the interval $[0,L]^2$

$$E(t)=E_{sf}(t)+E_{el}(t)=\frac{1}{L^2}\sum_{\vec{k}}\frac{1}{2}B(k)|\tilde{h}(\vec{k},t)|^2 \tag{A22}$$

with

$$B(k)=\gamma k^2-2E\frac{1+\sigma}{1-\sigma}\alpha^2k+\frac{2\gamma^2k^3}{E}(1-\sigma^2). \tag{A23}$$

This expression for $B(k)$ is different from a similar expression that has been suggested in [18]. From Eq. (A23) it can be seen, that the free energy of the film is decreased, i.e., $E(t)$ is negative, if the film possesses a periodic surface profile with a sufficiently large wavelength λ or small wave number k. On the other hand, $B(k)$ is positive if the condition

$$k>\frac{2E}{\gamma}\frac{1+\sigma}{1-\sigma}\alpha^2 \tag{A24}$$

is fulfilled. Insertion of the experimental parameters $\gamma\approx 2$ J/m^2 [19], $E\approx 100$ GPa [19], $p\approx 1$ GPa [19], $\sigma=0$, and $\alpha=(1-\sigma)p/E\approx 0.01$ in Eq. (A24) yields the condition $k>10^7$/m or equivalently $\lambda<630$ nm. Note that inserting a nonzero Poisson number σ would decrease the lateral deformation α and the RHS of Eq. (A24) and would thereby

expand the range of the wavelengths with positive $B(k)$. Since the experimentally observed surface morphologies on amorphous $Zr_{65}Al_{7.5}Cu_{27.5}$ films have a typical wave length of only $\lambda \approx 20$ nm [7–10], $B(k)>0$ holds at this wavelength. Hence, the free energy of the amorphous films is increased by the observed moundlike surface structure, $E(t)>0$. We estimate that the increase of the surface energy is at least one order of magnitude larger than the decrease of the elastic energy at the experimentally observed wavelength. Therefore, the moundlike surface structures seen on vapor deposited amorphous films cannot be interpreted as a consequence of an elastic instability.

[1] A.L. Barabasi and H.E. Stanley, *Fractal Concepts in Surface Growth* (Cambridge University Press, Cambridge, UK, 1995); W.M. Tong and R.S. Williams, Annu. Rev. Phys. Chem. **45**, 401 (1994); J. Krug, Adv. Phys. **46**, 139 (1997); M. Marsili, A. Maritan, F. Toigo, and J.R. Banavar, Rev. Mod. Phys. **68**, 963 (1996).

[2] D.E. Wolf and J. Villain, Europhys. Lett. **13**, 389 (1990).

[3] J. Villain, J. Phys. I **1**, 19 (1991).

[4] S. Das Sarma and P. Tamborenea, Phys. Rev. Lett. **66**, 325 (1991).

[5] Z.-W. Lai and S. Das Sarma, Phys. Rev. Lett. **66**, 2348 (1991).

[6] M. Siegert and M. Plischke, Phys. Rev. E **50**, 917 (1994).

[7] B. Reinker, M. Moske, and K. Samwer, Phys. Rev. B **56**, 9887 (1997).

[8] S.G. Mayr, M. Moske, and K. Samwer, Phys. Rev. B **60**, 16 950 (1999).

[9] S.G. Mayr, M. Moske, and K. Samwer, Mater. Sci. Forum **343-346**, 221 (1999).

[10] S.G. Mayr, M. Moske, and K. Samwer, *The Growth of Vapor Deposited Amorphous ZrAlCu-Alloy Films: Experiment and Simulation*, edited by H.-J. Bungartz, R.H.W. Hoppe, and C. Zenger, Lectures on Applied Mathematics (Springer, Berlin, 2000), p. 233.

[11] T. Salditt, T.H. Metzger, J. Peisl, B. Reinker, M. Moske, and K. Samwer, Europhys. Lett. **32**, 331 (1995).

[12] M. Raible, S.J. Linz, and P. Hänggi, Phys. Rev. E **62**, 1691 (2000).

[13] S.J. Linz, M. Raible, and P. Hänggi, Lect. Notes Phys. **557**, 473 (2000).

[14] M. Raible, S.G. Mayr, S.J. Linz, M. Moske, P. Hänggi, and K. Samwer, Europhys. Lett. **50**, 61 (2000).

[15] M. Kardar, G. Parisi, and Y.-C. Zhang, Phys. Rev. Lett. **56**, 889 (1986).

[16] N.J. Shevchik, J. Non-Cryst. Solids **12**, 141 (1973).

[17] W.W. Mullins, J. Appl. Phys. **28**, 333 (1957).

[18] M. Rost, e-print cond-mat/0004194.

[19] M. Moske, habilitationsschrift, Universität Augsburg, 1997.

[20] P. Manneville, in *Propagation in System Far from Equilibrium*, Vol. 41 of Springer Series in Synergetics, edited by Jose E. Wesfreid *et al.* (Springer, Berlin, 1988), p. 265; I. Procaccia, M.H. Jensen, V.S. L'vov, K. Sneppen, and R. Zeitak, Phys. Rev. A **46**, 3220 (1992); C. Jayaprakash, F. Hayot, and R. Pandit, Phys. Rev. Lett. **71**, 12 (1993); M. Rost and J. Krug, Physica D **88**, 1 (1995); J.T. Drotar, Y.-P. Zhao, T.-M. Lu, and G.-C. Wang, Phys. Rev. E **59**, 177 (1999).

[21] R.J. Asaro and W.A. Tiller, Metall. Trans. **3**, 1789 (1972).

[22] M.A. Grinfeld, Dokl. Akad. Nauk SSSR **265**, 836 (1982); **290**, 1358 (1986); M.A. Grinfeld, Sov. Phys. Dokl. **31**, 831 (1986); Europhys. Lett. **22**, 723 (1993).

[23] D.J. Srolovitz, Acta Metall. **37**, 621 (1989).

[24] M. Raible, *Stochastische Feldgleichungen für Amorphes Schichtwachstum*, dissertation, Universität Augsburg (Shaker Verlag, Aachen, 2000).